Volume 1 | Number 1 | Jan 2013 | Pages 1–100

Nanoscale

www.rsc.org/nanoscale

ROYAL SOCIETY OF CHEMISTRY

ROYAL SOCIETY OF CHEMISTRY

www.rsc.org/nanoscale

Nanoscale

PAPER

Nanoparticle Distribution during Systemic Inflammation is Size-Dependent and Organ-Specific

K.-H. Chen[a]†, D. J. Lundy[a]†, E.K.-W. Toh[a], C.-H. Chen[a], C. Shih[a], P. Chen[b], H.-C. Chang[c], J. J. Lai[d], P. S. Stayton[d], A. S. Hoffman[d] and P. C.-H. Hsieh[a,d]

This study comprehensively investigates the changing biodistribution of fluorescent-labelled polystyrene latex bead nanoparticles in a mouse model of inflammation. Since inflammation alters systemic circulatory properties, increases vessel permeability and modulates the immune system, we theorised that systemic inflammation would alter nanoparticle distribution within the body. This has implications for prospective nanocarrier-based therapies targeting inflammatory diseases. Low dose lipopolysaccharide (LPS), a bacterial endotoxin, was used to induce an inflammatory response, and 20 nm, 100 nm or 500 nm polystyrene nanoparticles were administered after 16 hours. HPLC analysis was used to accurately quantify nanoparticle retention by each vital organ, and tissue sections revealed the precise locations of nanoparticle deposition within key tissues. During inflammation, nanoparticles of all sizes redistributed, particularly to the marginal zones of the spleen. We found that LPS-induced inflammation induces splenic macrophage polarisation and alters leukocyte uptake of nanoparticles, with size-dependent effects. In addition, spleen vasculature becomes significantly more permeable following LPS treatment. We conclude that systemic inflammation affects nanoparticle distribution by multiple mechanisms, in a size dependent manner.

[a.] Institute of Biomedical Sciences, Academia Sinica, 128 Sec. 2, Academia Rd. Taipei 115, Taiwan. Correspondence email: phsieh@ibms.sinica.edu.tw
[b.] Research Center for Applied Sciences, Academia Sinica, 128 Sec. 2, Academia Rd, Taipei 115, Taiwan.
[c.] Institute of Atomic and Molecular Sciences, Academia Sinica, No. 1, Roosevelt Rd., Sec. 4, Taipei 105, Taiwan
[d.] Department of Bioengineering, University of Washington, Box 355061 N107 William H. Foege Building, 3720 15th Ave NE, Seattle, WA 98195, USA
† These authors should be considered as joint first author.
Electronic Supplementary Information (ESI) available: IF images of brain and heart, low magnification of spleen, mouse heart rate and blood pressure post-LPS. See DOI: 10.1039/x0xx00000x

Introduction

Nanoparticles, a convergence of nanotechnology and biomaterials, have been widely used in the biomedical field over the past decades in areas ranging from drug delivery[1,2] and tissue engineering[3,4] to molecular imaging[5,6], with great potential for translational medicine.[7] Due to the rapid development of new analytical techniques and materials, it is important to comprehend how nanoparticle characteristics such as size, shape, surface charge and conjugated functional groups may affect the treatment efficacy of nanoparticle-based therapies. There have been an increasing number of studies reporting that these physical and chemical properties govern cellular uptake, toxicity, biodistribution, retention and clearance of nanoparticles flowing systemic administration.[8–10] Understanding how nanoparticles are taken up, distributed and excreted is essential if we are to optimise their therapeutic effects. This is particularly relevant in disease states which affect normal physiological properties such as blood pressure and vascular permeability, as well as those which alter the immune system.

Many studies have demonstrated that particle size and shape greatly affect the transport and fate of the particle within the body.[11–14] As a general rule, nanoparticles of around 10 nm in diameter can be excreted by the kidney through glomerular filtration.[5,15] Larger nanoparticles (> 1,000 nm) distribute primarily in the capillaries of the liver and lungs, sometimes causing microemboli. Medium-sized nanoparticles (10-300 nm) tend to accumulate in the liver, spleen, lymph nodes and bone marrow due to these organs containing large numbers of macrophages.[16] Nanoparticles of less than 100 nm can escape systemic circulation through fenestrations in the endothelial lining.[11,17] Nanoparticles of larger than 500 nm can be phagocytosed by macrophages, whereas smaller nanoparticles can be endocytosed by professional phagocytic or non-phagocytic cells.[11,18,19] Pathological conditions usually cause microenvironmental changes at specific injury sites, thus affecting nanoparticle distribution. For example, most solid tumours have defective vasculature and may also produce various growth factors that can enhance vascular permeability. Macromolecules or nanoparticles therefore pass more readily into the tumour tissue through a leaky tumour vasculature, and are then retained in the tumour bed due to their larger size and poor lymphatic drainage.[20,21] This process is known as the enhanced permeability and retention (EPR) effect. It also has been demonstrated that nanoparticles (< 100 nm) more effectively penetrate through leaky tumour vasculature and into the surrounding cancer cells.[22]
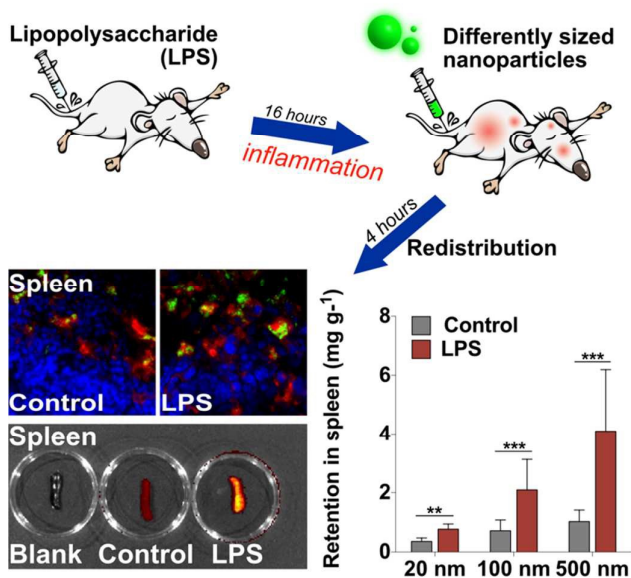
Scheme 1. Schematic summary of the investigation carried out. Polystyrene nanoparticle distribution following inflammation was assessed by HPLC, IVIS and immunofluorescence staining of key organs and tissues.

Systemic inflammation can be triggered by a variety of infectious and non-infectious conditions and is known to alter blood flow, increase vascular permeability and activate the immune system.[23] We theorised that an inflammatory condition might modify the distribution profile of systemically injected nanoparticles. In order to develop targeted nanomedicines for treatment of inflammatory diseases, the size-dependent distribution of nanoparticles needs to be well studied. This information can provide guidance for appropriate particle selection under different disease conditions. Thus, we aimed to comprehensively study the biodistribution of polystyrene nanoparticles under inflammatory conditions, as well as investigating the underlying mechanisms behind nanoparticle redistribution during inflammation.

Experimental Section

Animal Experimentation

The Experimental Animal Committee, Academia Sinica, Taiwan approved all animal experimental procedures. 8-week-old male FVB mice, used for all investigations, were purchased from the National Laboratory Animal Center, Taiwan and were stored with a 12-hour night/day cycle and free access to food and water.

Lipopolysaccharide (LPS) and Nanoparticle Administration

Lipopolysaccharide from *E.coli* 0111:B4 (Sigma L4391, USA) was administered via lateral tail vein (5 mg kg-1) and mice were returned to their cages with free access to food and water for 16 hours. Unmodified, fluorescent carboxylated polystyrene latex bead nanoparticles (Invitrogen FluoSpheres, yellow/green) with uniform diameters of 20, 100, and 500 nm were injected (5 mg kg-1) slowly via lateral tail vein. These

nanoparticles are non-degradable, thus excluding resorption as a variable.

Fluorescent Dye Extraction and HPLC Quantification of Nanoparticle Retention

Four hours following nanoparticle injection, mice were sacrificed by cervical dislocation. Major organs and tissues (brain, heart, lungs, liver, spleen, kidneys, skin, fat, blood and urine) were rapidly harvested. For HPLC analysis, the harvested tissues were washed with warm PBS, dried, cut into several ~100 mg pieces and weighed. De-ionised water (0.5 ml) was added to each sample, followed by thorough homogenisation using MagNA Lyser instrument with zirconia beads (Roche, Mannheim, Germany). Homogenised samples were thoroughly mixed with *o*-xylene (0.5 ml) for fluorescent dye extraction and sonicated for a total of 2 minutes and then incubated at -80 ˚C for 30 minutes. After thawing, samples were centrifuged at 14,000 rpm for 30 minutes and supernatant, containing the extracted fluorescent dye, was withdrawn, diluted, and subjected to HPLC analysis. HPLC was carried out using a Waters e2695 Separation Module and Waters 2475 FLR Detector, (USA). An X-Bridge C18 column (250 × 4.6 mm, 5 µm, Waters, USA) was used at 40 ˚C and the fluorescence detector was set to an excitation wavelength of 505 nm and emission wavelength of 515 nm. The mobile phase consisted of methanol and de-ionised water (77:23, v/v) with a flow rate of 1 ml min^{-1}. HPLC standards were measured by sampling serial dilutions of 4.0 to 0.0019531 µg ml^{-1} nanoparticles. For standard solutions, the extraction procedures were identical to the protocol as described above. Standard curves were generated for each nanoparticle size and the extraction efficiency was checked for consistency between different tissues. Nanoparticle retention was assessed by "spiking" low (0.03125 µg ml^{-1}), medium (0.25000 µg ml^{-1}) and high (2.00000 µg ml^{-1}) concentrations of nanoparticles into liver tissue, then extracting the dye via the above methodology. The relative amount of nanoparticle retention in each sample was then calculated using standard curves.

Nanoparticle Characterisation

Nanoparticles were diluted to 10 µg ml^{-1} in ultra pure water or 10 mM Tris buffer pH 7.0 for hydrodynamic size and zeta potential determination by DLS and ELS respectively, using a Malvern ZetaSizer ZS instrument. For TEM sizing, nanoparticles were deposited onto copper grids, stained with PTA (2 % w/v) and dried overnight. Please see ESI Fig. S3 for nanoparticle characterisation.

In Vivo Imaging System (IVIS)

An *IVIS* 200 system (Caliper Life Sciences, Massachusetts, USA) was used to observe the nanoparticle biodistribution in freshly collected tissues and organs.

Immunofluorescence Imaging

Samples were dehydrated for 6 hours in sucrose solution (15 % w/v) and then overnight in concentrated (30 % w/v) sucrose solution before being embedded in tissue freezing medium at -

20 ˚C and cryosectioned. Blood vessels were visualised using Alexa Fluor 647-conjugated anti-isolectin antibody (1:400, Invitrogen), and nuclei were counterstained with DAPI (1 mg ml^{-1}). Other antibodies used to identify splenic leukocytes were used as follows: CD68-AF647 (1:200, Biolegend), CD169-AF647 (1:200, Biolegend), CD209b-APC (1:200, eBioscience) at 4 ˚C overnight, and CD15 (1:200, Biolegend) overnight at 4 ˚C followed by AF647 secondary antibody for 1 hour at room temperature. F4/80 was stained using anti-F4/80 (1:200, BioRad) overnight at 4 ˚C followed by anti-Rat AF647 (1:400, Jackson ImmunoResearch). Images were captured on a Zeiss Axioscop microscope and processed with AxioVision software.

Flow Cytometric Analysis of Splenic Leukocytes

In order to quantify the percentage of splenic leukocytes containing nanoparticles under normal or inflammatory conditions, the spleen was freshly removed, broken apart and gently mashed through a 100 μm cell strainer to release cells. Suspended cells were briefly spun down at 500x g for 5 minutes, supernatant discarded and the pellet resuspended in ACK lysis buffer and incubated for 5 minutes at room temperature, neutralised with LG-DMEM (10 % FBS), before being washed again with DMEM-10 (9 ml). The pellet was collected, resuspended in PBS (3 ml) then incubated with antibodies at appropriate dilutions. Cells were then fixed in paraformaldehyde (2 % w/v). Flow cytometry was performed using a BD LSR II 15 colour flow cytometer. Blank control and LPS-treated spleens without nanoparticles or antibodies, as well as isotype controls for each antibody, were used to establish gating parameters that were then applied to all subsequent samples. Please see ESI Fig. S4 for antibodies and dilutions used in these experiments.

Assessment of Systemic Extravasation by Evans blue Assay

Vascular extravasation caused by LPS was assessed by injection of Evans blue dye (Miles assay), as previously described.[24] Evans blue in PBS (0.5 % w/v) was filter sterilised and injected by tail vein at a dose of 5 mg kg-1 and the animal was sacrificed by cervical dislocation after 30 minutes. Organs were quickly removed and washed, and 50-100 mg pieces were homogenised in formamide (500 μl), incubated at 55 ˚C overnight, and then centrifuged at 21,000x g for 15 minutes. Supernatant was measured in triplicate at 620 nm with background correction at 740 nm in a plate reader, with unknowns quantified from a standard curve of Evans blue in formamide and expressed as nanograms of dye per gram of tissue. Blank organs, without Evans blue, were used to establish a baseline.

Physiological Analyses

All physiological analyses were performed by independent staff in the Taiwan Mouse Clinic, Academia Sinica, Taiwan. 8 week old, male, FVB mice were used for all analyses (n = 5 per group). Blood pressure, heart rate and core body temperature were collected continuously for 30 minutes.

Data Handling, Image Processing and Statistical Analysis

Results, unless otherwise stated, are expressed as the mean ± standard error of the mean. Statistical analyses were performed using GraphPad Prism 6 software. 2-way ANOVA with Tukey's multiple comparison post-test was used to analyse HPLC data, flow cytometry data and Evans blue retention. We used t-test to compare nanoparticle recovery rates between KOH and homogenisation methods for each nanoparticle size and concentration. Results were considered statistically significant if P < 0.05, and levels of statistical significance are noted in figure legends where appropriate. Figures were assembled in Apple Keynote software and Affinity Designer (Mac). Linear adjustments to brightness were made to enable clearer visualisation of nanoparticles within tissue sections.

Results and Discussion

High-performance Liquid Chromatography Allows for Sensitive and Accurate Quantification of Nanoparticle Retention Within Tissues

We have previously shown that HPLC is a sensitive and precise method to quantify nanoparticle retention.[25] However, we have recently found that using alkaline chemical digestion to extract nanoparticle dye from tissues may accelerate the decay of the fluorescent dye. This subsequently reduces the effective recovery rate of fluorescent dye, resulting in an underestimated nanoparticle uptake by organs which disproportionately affects smaller nanoparticles. Therefore, we have developed an improved methodology where fluorescent dye is released under stable, neutral conditions by physical methods, followed by solvent-based extraction and separation of fluorescent dye. Using a combination of thorough
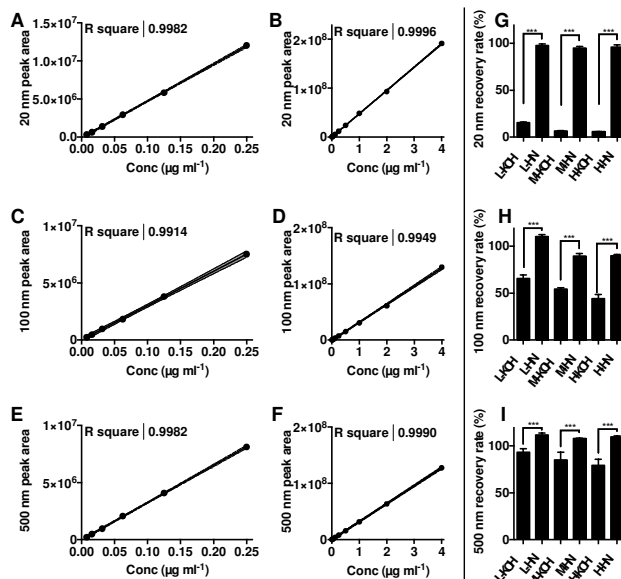
Fig. 1. Low concentration and high concentration standard curves for 20 nm, 100 nm and 500 nm fluorescent nanoparticles (A-F). Dotted lines show 95 % confidence limits. The recovery rate percentage using homogenisation (HN) and potassium hydroxide digestion (KOH) to extract low, medium and high (L, M, H) concentrations of nanoparticles is shown for each nanoparticle size in G-I. *** = P < 0.001.

homogenisation, sonication, freeze-thaw lysis and xylene extraction, we are able to achieve a fluorescent dye recovery rate of ≥ 90 % and an extremely low limit for detection and quantification (LOD 0.003 μg ml^{-1}, LOQ 0.009 μg ml^{-1}) for all nanoparticle sizes. HPLC analysis then allows for extremely accurate, consistent measurements of nanoparticle uptake. R-squared values of the calibration curves (Fig. 1(A-F)) are approximately 1, demonstrating a linear trend for the standard samples of each nanoparticle size. The recovery rate of 20 nm, 100 nm and 500 nm nanoparticles from tissue is superior when using the homogenisation (HN) method, rather than KOH digestion method (Fig. 1(G-I)), particularly for smaller nanoparticles. Recovery rates are size dependent due to the relative difficulty of lysing smaller nanoparticles and extracting the smaller volume of fluorescent dye which they contain. Larger nanoparticles are easier to lyse and contain much larger volumes of fluorescent dye, and typically show higher recovery

rates, as shown in our previous publication.[25] A recovery rate of 90-110 % is deemed acceptable for biological samples§.[26]

HPLC Analyses Reveals Organ-Specific, Size-Dependent Redistribution of Nanoparticles During a State of Inflammation

HPLC results (Fig. 2) show that, irrespective of nanoparticle size or LPS administration, the majority of systemically administered nanoparticles were retained by the lungs, liver and spleen. Distribution into other vital organs such as the brain and heart, or skin, muscle and fat tissue was less than 1 % in total, and were unaffected by LPS-induced inflammation. In healthy mice, most administered nanoparticles were retained by lungs, liver and spleen, as previously published.[25] Analysis of the blood shows that more than 99.5 % of the injected nanoparticles have been cleared from the
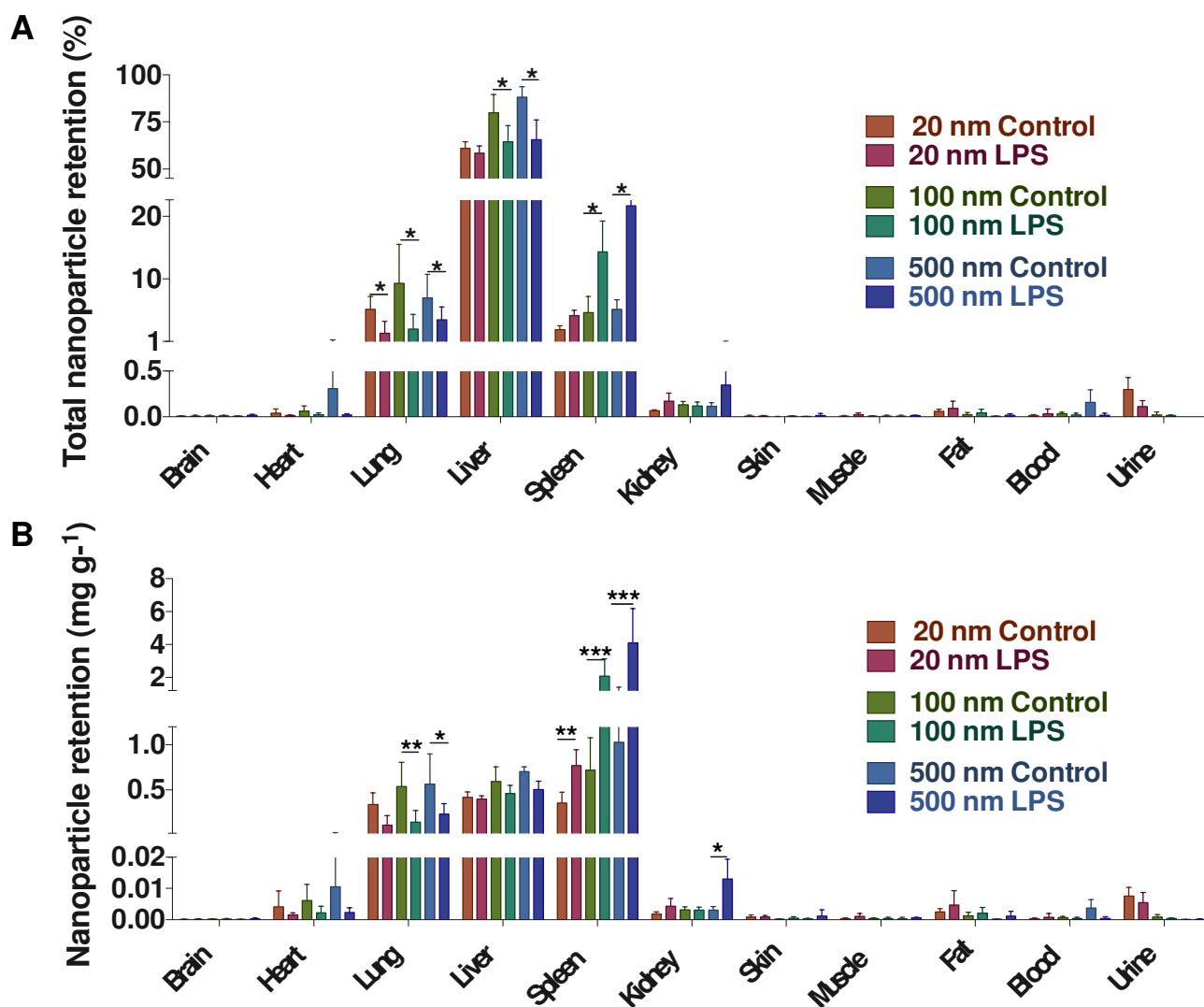
Fig. 2. HPLC analysis shows tissue and organ distribution of injected fluorescent nanoparticles in control or LPS-injected mice. (A) Percentage retention by each tissue. (B) Nanoparticle retention standardised by tissue weight. * = P < 0.05, ** = P < 0.01, *** = P < 0.001.

bloodstream four hours after administration. As expected, more 20 nm nanoparticles are found in the urine, since they may pass through the glomerulus, into the filtrate and eventually into the urine. Our deliberate use of non-degradable polystyrene nanoparticles eliminates resorption as a variable.

In healthy mice, nanoparticles were retained in the liver in proportion to the nanoparticle size (Fig. 2(A)). Although the lungs and spleen also appeared to show size-dependent accumulation, this effect was not statistically significant. HPLC analysis shows that considerable nanoparticle redistribution occurred in LPS-inflamed mice. In particular, the percentage of injected 100 nm and 500 nm nanoparticles retained by spleen increased markedly (four-fold), whilst the accumulation in the liver and lungs decreased by 30-40 %. We hypothesised that the spleen, which plays a vital role in the immune system, retains more nanoparticles during systemic inflammation, thus leading to the reduction of nanoparticle retention by other organs. Standardising nanoparticle distribution by expressing it according to the weight of each organ reveals a more balanced distribution of nanoparticles amongst the lungs, liver and spleen in healthy mice (Fig. 2(B)). Nanoparticle retention in the spleen was size dependent, with greater retention of larger nanoparticles. Following LPS-induced inflammation, a large increase in splenic nanoparticle retention is seen. Surprisingly, increased retention of 500 nm nanoparticles was detected in the LPS-treated kidneys, although the total amount retained is very low.

In-vivo Imaging System (IVIS) Analysis Confirms Nanoparticle Redistribution Following LPS-Induced Inflammation

Various techniques have been previously used to study nanoparticle distribution. However, the detection depth, sensitivity, and resolution may limit the ability to detect amounts of nanoparticles embedded in deeper regions of the organ or tissues. Thus, we have utilised multiple methods to measure nanoparticle distribution, allowing us to precisely quantify and locate nanoparticles within different organs. In
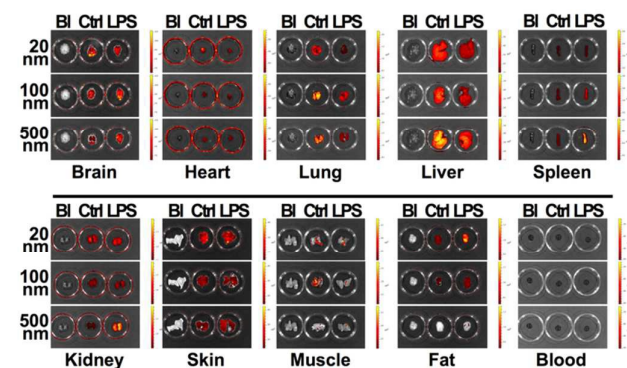

Fig. 3. *In vivo* imaging system (IVIS) images of organs from control or LPS-injected mice. Organs from blank (BI; no nanoparticles), control (Ctrl), and LPS-treated (LPS) mice are shown. Excitation wavelength 505 nm, emission 515 nm.

large agreement with HPLC results, IVIS images (Fig. 3) showed that the fluorescence signal of the spleen increased significantly following LPS-induced inflammation. A decreased fluorescence signal after LPS administration is also clearly visible in the lungs and liver. Again, the kidneys show an increased retention of 500 nm nanoparticles under inflammatory conditions. Visual comparison between different organs is not possible using IVIS, since vastly different levels of nanoparticle uptake required different exposure lengths for each group of organs. Larger nanoparticles also contain more dye and thus produce a stronger signal than 20 nm nanoparticles, and thus is not necessarily indicative of a larger amount of nanoparticle uptake. Blank (BI) samples, with no injected nanoparticles, are presented to demonstrate a lack of autofluorescence at the shown exposure length.

IVIS is depth limited, and measurable intensity depends on the tissue type and the source of the fluorescence, leading to more variability in results.[25] Our previous study also demonstrated that IVIS has a signal saturation problem when quantifying retention of nanoparticles. HPLC is an overall superior method for quantifying nanoparticle retention, with better sensitivity, accuracy and linearity. Thus, we consider IVIS as useful for comparing the same fluorescence source within the same tissue, or within living animals, rather than a suitable way to accurately compare biodistribution between different tissues.

Histological Analysis Reveals Specific Locations of Nanoparticle Retention Under Normal and Inflammatory Conditions.

HPLC is a more sensitive and precise method to quantify nanoparticle retention than IVIS, but it requires destruction of the tissue and only measures total nanoparticle retention. Therefore, in order to examine the distribution of nanoparticles within the tissues more closely, organs were collected and prepared for cryosectioning and immunofluorescence analysis. Isolectin, a marker for endothelial cells, was used to demarcate blood vessels (red) whereas fluorescent nanoparticles are detectable in the green channel. Please note that visual comparison between nanoparticles of different sizes is not possible, since larger nanoparticles contain more fluorescent dye and require a shorter exposure length. Thus, immunofluorescence images are for comparison of nanoparticle location within the tissues, rather than assessment of their relative numbers. Images shown in Fig. 4[‡] show that in the lung tissue, plentiful nanoparticles were observed in both normal and LPS-treated mice, mainly outside of blood vessels. The reduction in nanoparticle retention during inflammation measured by HPLC is not readily apparent in the histological analysis. It appears that nanoparticles in the liver were evenly distributed over the entire tissue section, and nanoparticle accumulation was visibly decreased after LPS treatment. Conversely, nanoparticles in the spleen were confined mostly to the marginal zones (MZ) surrounding the white pulp (WP). Fewer particles were observed in the red pulp (RP). Isolectin staining shows that many nanoparticles of all sizes, although
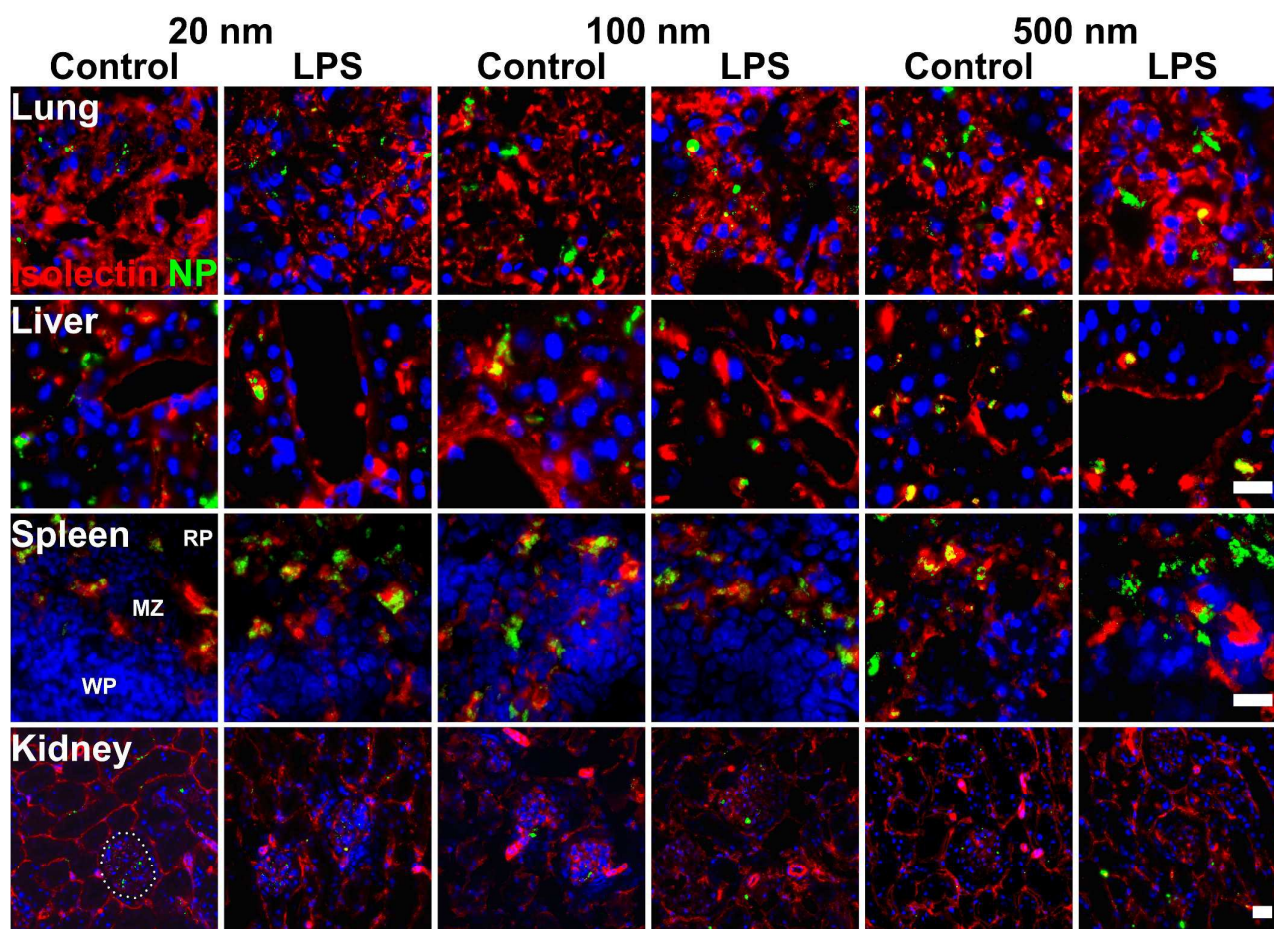
Fig. 4. Immunofluorescence images of major nanoparticle-retaining organs are shown, stained for isolectin (red). Nanoparticles are shown in green, nuclei (DAPI) in blue. The kidney glomerulus is encircled with a dotted white line. In the spleen, examples of the white pulp (WP), red pulp (RP), and marginal zones (MZ) are noted. Scale bars = 20 µm.

particularly 20 nm and 100 nm nanoparticles, are contained in close proximity to blood vessels. In the kidneys, 20 nm nanoparticles are contained mainly within the glomerulus of the kidneys, whereas larger particles are distributed in the glomerulus and the cortex. This corresponds to the larger number of 20 nm nanoparticles found in the urine. Nanoparticles in the brain (ESI - Fig. S1(A)) and heart (ESI - Fig. S1(B)) were rare, in agreement with HPLC analysis. Lower magnification images of the spleen showing nanoparticles accumulating in the marginal zones are available in ESI - Fig. S1(C).

The spleen has naturally permeable vasculature with endothelial fenestrations, which function as a sieve to filter foreign bodies from the blood. These are then rapidly taken up by tissue macrophages. Histological analysis of the spleen showed that most nanoparticles were deposited in the marginal zones, in agreement with previous studies.[27,28] LPS induces systemic inflammation via the toll-like receptor 4 (TLR4) signalling pathway[29] and the immune responses play a vital role in engulfment of foreign objects.[30,31] Since the spleen is considered as a reservoir of various immune cells[27], we sought to investigate the relationship between nanoparticles and splenic leukocytes further.

Investigation of Nanoparticle Uptake by Splenic Leukocytes During Inflammation.

We theorised that increased splenic retention of nanoparticles during inflammation might be due to their uptake by leukocytes. Immunofluorescence staining in Fig. 4 showed that the majority of nanoparticles were retained within the marginal zones, surrounding the white pulp, where many splenic leukocytes reside. Therefore, we utilised immunofluorescence imaging to assess colocalisation of nanoparticles and leukocytes, as shown in Fig. 5. Colocalisation in this instance may refer to uptake by leukocytes, or adherence to their surface. CD68^{+} cells, representing a broad spectrum of tissue macrophages, were visualised in large numbers throughout the entire spleen sections - in the white pulp, red pulp and marginal zones. CD68^{+} cell colocalisation with nanoparticles was common for 20 nm and 100 nm nanoparticles, but much less frequently observed for 500 nm nanoparticles. Any difference in the proportion of uptake between control and LPS-treated spleens is difficult to visualise[‡], but an increased total number of CD68^{+} cells, and an increased total number of nanoparticles is clearly visible.

CD169^{+} cells, representing metallophilic marginal zone macrophages, showed colocalisation, particularly with 100 nm and 500 nm nanoparticles. Interestingly, LPS-administered mice showed less nanoparticle colocalisation with CD169^{+} cells. CD209b^{+} cells, representing perifollicular marginal zone macrophages and dendritic cells, showed strong colocalisation for all nanoparticle sizes, although the absolute number of these cells in each spleen section appeared lower than other groups. An increase in nanoparticle colocalisation is visible for 100 nm nanoparticles, though less apparent for 500 nm nanoparticles. CD15^{+} cells, representing neutrophils, show no visible colocalisation for any nanoparticle size, regardless of LPS treatment and F4/80^{+} cells, representing red pulp macrophages show colocalisation for each group, but noticeably more with 500 nm nanoparticles.

In order to quantitate these findings, we took advantage of flow cytometry analysis to measure the number of leukocytes associated with fluorescent nanoparticles. Spleens were removed from control or LPS-treated mice, four hours after nanoparticle administration, then mashed, cells strained out, and cells stained for immune markers and subjected to flow cytometry. Results, shown in Fig. 6(A), indicate that many nanoparticles are indeed adhered to, or engulfed by, splenic leukocytes. 20 nm nanoparticles are highly taken up by all leukocyte subpopulations that were tested, apart from CD15^{+} cells, and LPS-induced inflammation did not alter 20 nm nanoparticle uptake for any of the cell populations examined.

100 nm nanoparticles were again taken up by all tested leukocyte populations, but a significant increase in uptake by CD15^{+} cells was measured during inflammatory conditions. 500 nm nanoparticles were generally taken up more poorly than smaller nanoparticles.
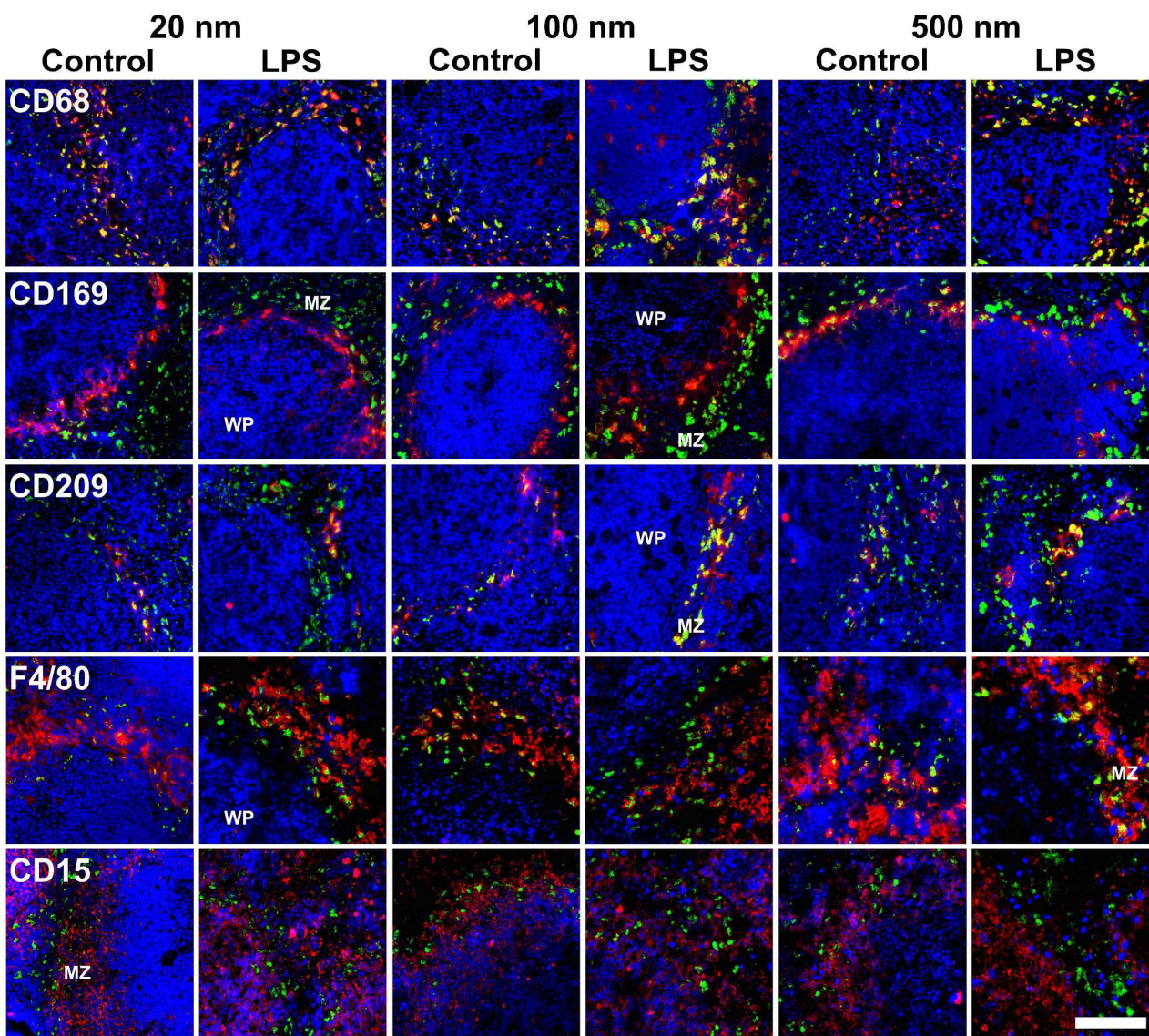
Fig. 5. Leukocyte colocalisation with fluorescent nanoparticles, stained by denoted markers in control or LPS-treated mice. Key features of spleen anatomy; the white pulp (WP) and marginal zone (MZ) are labelled for reference. Blue, DAPI; Red, denoted cell surface marker; Green, Nanoparticle. Scale bar = 100 μm

This corresponds to previous reports showing that nanoparticle uptake is size-dependent and drastically declines as particle size increases.[32,33] We also measured a significant increase in uptake of 500 nm nanoparticles by CD209b^{+} cells during inflammation. Interestingly, CD169^{+} cells took up fewer 500 nm nanoparticles after LPS. Fig. 6(D) shows that the number of each cell population extracted from the spleen did not change after LPS. Thus, observed differences must be attributed to a change in uptake of nanoparticles by leukocytes, rather than a change in the leukocyte population size itself. LPS is a well-known macrophage activator, inducing cells to release reactive oxygen species, nitric oxide and pro-inflammatory cytokines such as IL-6, Ccl2 and TNF-α.[23,34] Previous studies have reported that LPS treatment can abate phagocytic clearance of apoptotic cells, pathogens and erythrocytes by macrophages.[35–37] We measured a reduced uptake of 500 nm nanoparticles by splenic CD169^{+} cells, but there was no general inhibitory effect observed in our study. This is likely due to the relatively short time period between LPS administration and nanoparticle injection used in our study.

In addition, since LPS is a well-known stimulator of macrophage polarisation, we have analysed the effect of LPS administration on the splenic macrophage population. Live cells selected and then sorted by flow cytometry into CD45^{+}/CD11b^{+}/F4-80^{+}/Ly-6g^{+} and CD45^{+}/CD11b^{+}/F4-80^{+}/CD206^{+} populations, representing M1 and M2 macrophages respectively. The non-polarised (M0), macrophage population was also measured. Macrophages (M0/M1/M2) comprised 0.5-1.5 % of the total cells isolated from the spleen, and no change in total population size was observed following LPS treatment. These data, shown in Fig. 6(B-C) show that LPS indeed induces M1 macrophage polarization, which is in agreement with previously shown data.[38] Macrophage polarisation is evident by a decreased M0 population and increased M1 population in all LPS treatment groups (Fig. 6B). However, the M2 population remains unchanged in all groups (Fig. 6(B)). This is expected since M1 "killer" macrophages are implicated in the inflammatory response and the clearance of foreign compounds, whereas the M2 "healer" macrophage population is primarily concerned with tissue remodelling and repair. We observed few changes in nanoparticle uptake in either M1 or M2 macrophages following LPS administration, aside from a small increase in 500 nm nanoparticle uptake by M0 macrophages (Fig. 6C). Please note that the Y-axes vary because of the amount of fluorescent dye contained within differently sized nanoparticles. We conclude that although LPS strongly induces splenic macrophage polarization, this polarisation is not a significant factor in the increased nanoparticle uptake by the spleen.

Systemic Effects of LPS-Induced Inflammation Affect Nanoparticle Uptake.
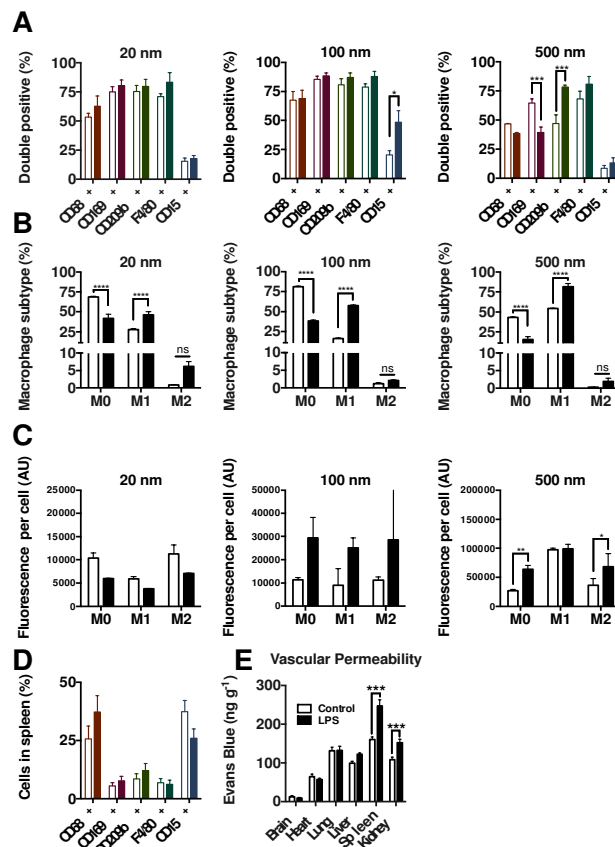

Fig. 6. (A-D) Flow cytometry analysis of colocalisation between isolated splenic leukocytes and injected fluorescent nanoparticles in control (clear bars) or LPS-treated (shaded bars) mice. (E) Extravasation following LPS-induced inflammation, as measured by organ-specific Evans blue retention.

Taking into account the altered uptake of nanoparticles by splenic leukocytes, we reasoned that these changes alone were not enough to ascribe all changes in biodistribution observed by HPLC analysis (Fig. 1), particularly for 20 nm nanoparticles. Therefore, we sought to better understand the physiological changes that occur after LPS administration. A moderate dose of 5 mg kg^{-1} LPS was sufficient to trigger an inflammatory response in mice, without causing lethality. Lethargy began two hours after LPS injection, and complete blood count analysis showed a typical response including a raised total white blood cell count, with lymphocytopaenia after 20 hours (ESI Fig. S2(B)). Physiological analyses showed that LPS-inflamed mice had a reduced heart rate, as well as reduced systolic and diastolic blood pressure, as shown in ESI Fig. S2(B) (supporting information). This is in agreement with previous studies.[34,39,40] In the marginal zones of the spleen, the blood leaves the terminal arterioles into open sinuses, the blood flow slows, and blood-borne particles are trapped with high efficiency.[28] In addition, a previous study has demonstrated that LPS significantly lowers splenic blood flow.[41] Taking the splenic anatomy into consideration, we speculate that these factors might contribute to increased retention of nanoparticles after LPS-induced inflammation.

LPS-Induced Inflammation Causes Increased Vascular Permeability in an Organ-Specific Manner.

LPS administration has been shown to induce systemic inflammation affecting multiple organs in mice. For example, systemic LPS administration, given at the same dose as in our study (5 mg kg -1), has been shown to induce inflammation of the brain via TNF-α release, as well as neurodegeneration[42]. However, we did not measure increased uptake of nanoparticles by the brain following LPS administration. Thus, even though the brain is profoundly affected by this systemic inflammatory condition, this may not manifest itself by increased nanoparticle uptake. In addition, systemic LPS administration in mice has been shown to induce renal damage[43], cardiomyopathy[44], and apoptosis/necrosis of liver tissues.[45] However, we detected few changes in these organs, aside from the liver where nanoparticle retention decreased following LPS administration. Therefore we conclude that LPS inflammation-driven changes in nanoparticle retention are organ specific.

Physiological changes such as a reduction in systemic blood flow rate, lowered heart rate and decreased blood pressure would likely affect nanoparticle deposition. However, these changes are systemic, and so would not explain increased retention by the spleen specifically. It has been reported previously that endotoxin-elicited inflammation increases vascular permeability, thus lowering the sieving effect of fenestrated endothelium.[46] Therefore, we used an Evans blue extravasation assay (Miles assay) to measure systemic vascular permeability 16 hours after LPS administration.[24] After injection into the blood stream, Evans blue rapidly binds to albumin and remains restricted within intact blood vessels. However, if blood vessels are leaky, damaged or otherwise compromised, Evans blue will be able to enter tissues. Evans blue was allowed to circulate for 30 minutes before organs were rapidly collected and dye extracted and quantified. Results shown in Fig. 6(E) reveal that the Evans blue dye content of the spleen and kidneys increased significantly during LPS-induced inflammation, but the brain, heart, lungs and liver were unaffected. Images of Evans blue stained organs are shown in ESI Fig. S2(A). This shows that the LPS-induced inflammatory condition alters vascular permeability in the spleen in a disproportionate manner to other organs. This would explain the increased uptake of 20 nm nanoparticles but it is unlikely that blood vessels would become so permeable as to allow free passage of larger 100 nm or 500 nm nanoparticles. Thus, it is likely that increased nanoparticle retention by tissues during inflammation is size dependent and affected by multiple mechanisms, with smaller nanoparticles passing through inflamed blood vessel fenestrations and larger nanoparticles being increasingly sequestered by leukocytes.

One limitation of these findings is that they are likely to be material dependent to some extent. We have shown that splenic blood vessel permeability increases during LPS-induced inflammation (Fig. 6(E)), which should be applicable to many nano-sized materials. However, the cellular uptake of nanoparticles, particularly by immune cells, is known to be dependent on their physiochemical properties[18], and thus these results may not be relevant to every nano-carrier material. In addition, since intravenously injected LPS induces a systemic inflammatory condition with widespread effects in multiple organs, extrapolation of these findings to local tissue inflammation should be undertaken with caution. Local tissue damage with necrosis and oxidative stress manifests itself through the enhanced permeability and retention (EPR) effect, whereas LPS induced inflammation is based on systemic cytokine release and vascular smooth muscle relaxation. Similarly, LPS has distinct and profound effects on the immune system, including the polarisation of macrophages, and thus may not reflect all varieties of systemic inflammation.

Conclusions

An inflammatory condition affects nanoparticle biodistribution in a size-dependent, organ-specific manner by several mechanisms. During LPS-induced inflammation, the spleen retains dramatically more nanoparticles of all sizes. We have found that LPS-induced inflammation significantly increases the permeability of splenic blood vessels, allowing increased extravasation of 20 nm nanoparticles. However, these small nanoparticles are taken up by splenic leukocytes at the same rate during normal and inflammatory conditions. On the other hand, larger nanoparticles are increasingly colocalised with splenic leukocytes during LPS-induced inflammation. In addition, LPS administration induces polarisation of splenic macrophages, tending towards the M1 subtype. We hope that these results will provide new insights into nanoparticle biodistribution and allow for improved development of targeted therapies during inflammatory conditions.

Acknowledgements

Notes and references

‡ Since larger nanoparticles contain more fluorescent dye than smaller nanoparticles, and require different exposure lengths, immunofluorescence images should be considered as a tool for qualitative analysis of nanoparticle location within tissues.

§ Recovery values calculated as greater than 100 % are attributed to slight differences in the gradient of the standard curve. We did not observe any autofluorescence at the described wavelengths and retention time in any blank samples during our experimentation. All recovery rates in our study are within the ideal range of 90-110 %, used by the US FDA for QC verification.

1 S. Sengupta, D. Eavarone, I. Capila, G. Zhao, N. Watson, T. Kiziltepe and R. Sasisekharan, *Nature*, 2005, **436**, 568–572.
2 K. A. Woodrow, Y. Cu, C. J. Booth, J. K. Saucier-Sawyer, M. J. Wood and W. M. Saltzman, *Nat. Mater.*, 2009, **8**, 526–533.
3 A. Ito, E. Hibino, C. Kobayashi, H. Terasaki, H. Kagami, M. Ueda, T. Kobayashi and H. Honda, *Tissue Eng.*, 2005, 11, 489–496.
4 S. Sarkar, G. Y. Lee, J. Y. Wong and T. A. Desai, *Biomaterials*, 2006, **27**, 4775–4782.
5 H. S. Choi, W. Liu, P. Misra, E. Tanaka, J. P. Zimmer, B. Itty Ipe, M. G. Bawendi and J. V Frangioni, *Nat. Biotechnol.*, 2007, **25**, 1165–1170.
6 S. Lee, E. J. Cha, K. Park, S. Y. Lee, J. K. Hong, I. C. Sun, S. Y. Kim, K. Choi, I. C. Kwon, K. Kim and C. H. Ahn, *Angew. Chemie - Int. Ed.*, 2008, **47**, 2804–2807.
7 E. Lavik and H. von Recum, *ACS Nano*, 2011, **5**, 3419–3424.
8 S. D. Li and L. Huang, in *Molecular Pharmaceutics*, 2008, vol. 5, pp. 496–504.
9 H. S. Choi, W. Liu, F. Liu, K. Nasr, P. Misra, M. G. Bawendi and J. V Frangioni, *Nat. Nanotechnol.*, 2010, **5**, 42–47.
10 C. H. J. Choi, J. E. Zuckerman, P. Webster and M. E. Davis, *Proc. Natl. Acad. Sci. U. S. A.*, 2011, **108**, 6656–6661.
11 S. Mitragotri and J. Lahann, *Nat. Mater.*, 2009, **8**, 15–23.
12 C. He, Y. Hu, L. Yin, C. Tang and C. Yin, *Biomaterials*, 2010, **31**, 3657–3666.
13 K. Yaehne, A. Tekrony, A. Clancy, Y. Gregoriou, J. Walker, K. Dean, T. Nguyen, A. Doiron, K. Rinker, X. Y. Jiang, S. Childs and D. Cramb, *Small*, 2013, **9**, 3118–3127.
14 X. Huang, L. Li, T. Liu, N. Hao, H. Liu, D. Chen and F. Tang, *ACS Nano*, 2011, **5**, 5390–5399.
15 M. L. Schipper, G. Iyer, A. L. Koh, Z. Cheng, Y. Ebenstein, A. Aharoni, S. Keren, L. a. Bentolila, J. Li, J. Rao, X. Chen, U. Banin, A. M. Wu, R. Sinclair, S. Weiss and S. S. Gambhir, *Small*, 2009, **5**, 126–134.
16 R. Weissleder, M. Nahrendorf and M. J. Pittet, *Nat. Mater.*, 2014, **13**, 125–38.
17 M. Gaumet, A. Vargas, R. Gurny and F. Delie, *Eur. J. Pharm. Biopharm.*, 2008, 69, 1–9.
18 R. C. May and L. M. Machesky, *J. Cell Sci.*, 2001, **114**, 1061–1077.
19 J. Rejman, V. Oberle, I. S. Zuhorn and D. Hoekstra, *Biochem. J.*, 2004, **377**, 159–169.
20 H. Maeda, *Bioconjug. Chem.*, 2010, 21, 797–802.
21 J. Fang, H. Nakamura and H. Maeda, *Adv. Drug Deliv. Rev.*, 2011, 63, 136–151.
22 C. Wong, T. Stylianopoulos, J. Cui, J. Martin, V. P. Chauhan, W. Jiang, Z. Popovic, R. K. Jain, M. G. Bawendi and D. Fukumura, *Proc. Natl. Acad. Sci. U. S. A.*, 2011, **108**, 2426–2431.
23 J. E. Juskewitch, J. L. Platt, B. E. Knudsen, K. L. Knutson, G. J. Brunn and J. P. Grande, *Sci. Rep.*, 2012, **2**, 918.
24 M. Radu and J. Chernoff, *J. Vis. Exp.*, 2013, e50062.
25 W.-Y. Liao, H.-J. Li, M.-Y. Chang, A. C. L. Tang, A. S. Hoffman and P. C. H. Hsieh, *Nanoscale*, 2013, **5**, 11079–11086.
26 A. J. Reason, *Methods Mol. Biol.*, 2003, **211**, 181–194.
27 P. Aichele, J. Zinke, L. Grode, R. a Schwendener, S. H. E. Kaufmann and P. Seiler, *J. Immunol.*, 2003, **171**, 1148–1155.
28 M. Demoy, J. P. Andreux, C. Weingarten, B. Gouritin, V. Guilloux and P. Couvreur, *Pharm. Res.*, 1999, **16**, 37–41.
29 J. E. Juskewitch, B. E. Knudsen, J. L. Platt, K. A. Nath, K. L. Knutson, G. J. Brunn and J. P. Grande, *Am. J. Pathol.*, 2012, **180**, 32–40.
30 C. Nathan, *Nature*, 2002, **420**, 846–852.
31 M. Karin and F. R. Greten, *Nat. Rev. Immunol.*, 2005, **5**, 749–759.
32 T. Dos Santos, J. Varela, I. Lynch, A. Salvati and K. A. Dawson, *Small*, 2011, **7**, 3341–3349.
33 L. Leclerc and W. Rima, *Inhal. Toxicol.*, 2012, **9**, 580–588.
34 D. T. Skelly, E. Hennessy, M. A. Dansereau and C. Cunningham, *PLoS One*, 2013, **8**, 1–20.
35 S. N. Vogel, S. T. Marshall and D. L. Rosenstreich, *Infect. Immun.*, 1979, **25**, 328–336.
36 Y. Zhou, Y. Yang, G. Warr and R. Bravo, *J. Leukoc. Biol.*, 1999, **65**, 265–269.
37 X. Feng, T. Deng, Y. Zhang, S. Su, C. Wei and D. Han, *Immunology*, 2011, **132**, 287–295.
38 H. L. Herd, K. T. Bartlett, J. a. Gustafson, L. D. McGill and H. Ghandehari, *Biomaterials*, 2015, **53**, 574–582.
39 S. Ehrentraut, S. Frede, H. Stapel, T. Mengden, C. Grohé, J. Fandrey, R. Meyer and G. Baumgarten, *Arterioscler. Thromb. Vasc. Biol.*, 2007, **27**, 2170–2176.
40 J. a. Nemzek, K. M. S. Hugunin and M. R. Opp, *Comp. Med.*, 2008, **58**, 120–128.
41 E. Weitzberg, A. Hemsén, A. Rudehill, A. Modin, M. Wanecek and J. M. Lundberg, *Br. J. Pharmacol.*, 1996, **118**, 617–626.
42 L. Qin, X. Wu, M. L. Block, Y. Liu, G. R. Breese, J.-S. Hong, D. J. Knapp and F. T. Crews, *Glia*, 2007, **55**, 453–462.
43 P. N. Cunningham, H. M. Dyanov, P. Park, J. Wang, K. a Newell and R. J. Quigg, *J. Immunol.*, 2002, **168**, 5817–5823.
44 K. V Ramana, M. S. Willis, M. D. White, J. W. Horton, J. M. Dimaio, D. Srivastava, A. Bhatnagar and S. K. Srivastava, *Circulation*, 2006, **114**, 1838–1846.
45 J. Zhong, I. V. Deaciuc, R. Burikhanov and W. J. S. De Villiers, *Biochim. Biophys. Acta - Mol. Basis Dis.*, 2006, **1762**, 468–477.
46 S. J. Jeong, S. H. Han, C. O. Kim, J. Y. Choi and J. M. Kim, *Crit. Care*, 2013, **17**, R97.